The modification of molybdenum nitrides: the effect of the second metal component

Y. Li [b,*], Y. Zhang [a], R. Raval [b], C. Li [a], R. Zhai [a] and Q. Xin [a]

[a] *State Key Laboratory of Catalysis, Dalian Institute of Chemical Physics, Chinese Academy of Sciences, Dalian 116023, PR China*

[b] *Leverhulme Centre for Innovative Catalysis and Interdisciplinary Research Centre in Surface Science, Liverpool University, Liverpool L69 3BX, UK*

E-mail: yxli@liverpool.ac.uk

Received 24 June 1997; accepted 1 September 1997

A set of Mo_2N-based bimetallic catalysts with high surface area around 140 m^2/g have been successfully prepared from precursors obtained using the coprecipitation method. Both the precursors and the end-catalysts were characterized using scanning electron microscopy (SEM) and X-ray diffraction (XRD). The nitriding processes were monitored by differential thermal analysis (TDA). The catalytic properties of Co–Mo bimetallic catalyst under medium pressure (3.0 MPa) are much better for the hydrodenitrogenation of pyridine than those of pure γ-Mo_2N and a commercially used sulfided $CoMo/Al_2O_3$ catalyst. The introduction of the second metal component has been shown to disrupt the morphology of the nitride phase with a greater concentration of (111) planes being present compared to (200) planes, a situation that is reversed compared to γ-Mo_2N.

Keywords: catalysis, nitride, HDN, XRD, SEM, TDA, coprecipitation, molybdenum, cobalt, zirconium, cerium, bimetallic, MoO_3, γ-Mo_2N

1. The synthesis of the catalysts

It is well known that early transition metal nitrides and carbides possess excellent catalytic properties in reactions such as CO hydrogenation [1,2], ammonia synthesis [3], hydrotreating [4–6], isomerization [7,8], freon disposal [9], and automobile exhaust catalysis [10], in some cases surpassing the properties of the group VIII noble metal catalysts. However, the preparation of these materials with high surface area is rather demanding [11], which seriously limits their application for future industrial use [12,13]. In order to tackle this problem, we have introduced a second metal component into molybdenum nitride to make bimetallic nitrides, which involve an easier preparation method, and, at the same time, display good catalytic properties for the hydrodesulfurization and hydrodenitrogenation reactions.

The catalyst precursors were prepared by coprecipitation. Titanium, cerium, zirconium and cobalt were chosen as the second metals introduced into molybdenum nitride. A soluble salt containing the metal of each second component was mixed with ammonium heptamolybdate in an aqueous solution, and was evaporated in a water-bath and then dried at 393 K for 2 h, followed by calcination at 773 K for 3 h to obtain the precursor. The amount of the soluble salt was so decided as to make the oxide (or salt in the case of Ti) of the second metal to be 3 wt% of the obtained precursor. The soluble salts and the resultant oxides (salt) are: titanium, $Ti(SO_4)_2$ and $TiO(SO_4)$; cerium, $Ce(NO_3)_4$ and CeO_2; zirconium, $Zr(NO_3)_4$ and ZrO_2; cobalt, $Co(NO_3)_4$ and CoO. The precursor was then temperature-programmed nitrided (TPN) using the method described elsewhere [14]. The synthetic conditions and the physical properties of the bimetallic catalysts are listed in table 1.

2. The catalytic properties

All the obtained bimetallic catalysts were tested for the hydrodenitrogenation of pyridine, and, in comparison, the activities of γ-Mo_2N and a commercially used sulfided $CoMo/Al_2O_3$ catalyst were also tested. 0.5 g of each catalyst in the form of 20–40 mesh particles was loaded in a stainless steel reactor which was enclosed in a furnace. Each sample was pretreated in 3.0 MPa of H_2 at 673 K for 2 h before the catalytic reaction run. The $CoMo/Al_2O_3$ catalyst was sulfided at 673 K with a mixture of 10% H_2S/H_2 for 2 h. The reactant was composed of 89 wt% *n*-hexane (solvent), 10 wt% cyclohexane (internal standard) and 1 wt% pyridine, and was fed by a syringe pump. The liquid hourly space velocity (LHSV) was 12 h^{-1}, and the H_2 to liquid volume ratio was 300. The reaction was carried out at 573 K with a H_2 pressure of 3.0 MPa. The products were analyzed by gas chromatography using a 60 m fused silica capillary column and a flame ionization detector.

Figure 1 compares the conversion (CON) and the

* To whom correspondence should be addressed.

© J.C. Baltzer AG, Science Publishers

Table 1
The synthetic conditions of the bimetallic catalysts and their BET surface areas

Catalyst code	Precursor weight (g)	Heating rate (K/min)	Space velocity of NH_3 (h^{-1})	Final nitriding temperature (K)	S_{BET} (m^2/g)
TiMoN	5	1	17000	953	154
CoMoN	5	1	17000	882	148
ZrMoN	5	3	17000	973	132
CeMoN	5	1	17000	938	130
γ-Mo_2N	3	1	37000	973	140

denitrogenation (DEN) of pyridine as a function of on-stream time. CON is defined as the total percentage of pyridine converted, and DEN as the percentage of products which are nitrogen-free. Initially all the bimetallic catalysts, except Co–Mo, show high activities in terms of both CON (over 80%) and DEN (over 70%), however the activities deteriorate gradually (figures 1a–1c) with increasing on-stream time. In contrast the Co–Mo catalyst shows lower activity initially (63% CON and 50% DEN), which increases steadily till 3 h on stream and plateaus after 3.5 h (figure 1d). γ-Mo_2N shows reasonable activity, initially 58% CON and 35% DEN, which gradually decreases with on-stream time so that after ca. three and a half hours the activity stabilizes at 39% CON and 17% DEN (figure 1e). The activity of the commercially used sulfided $CoMo/Al_2O_3$ catalyst under these experimental conditions is comparable to that of γ-Mo_2N: initially 55% CON and 35% DEN, and stabilises at 39% CON and 16% DEN after three and a half hours (figure 1f).

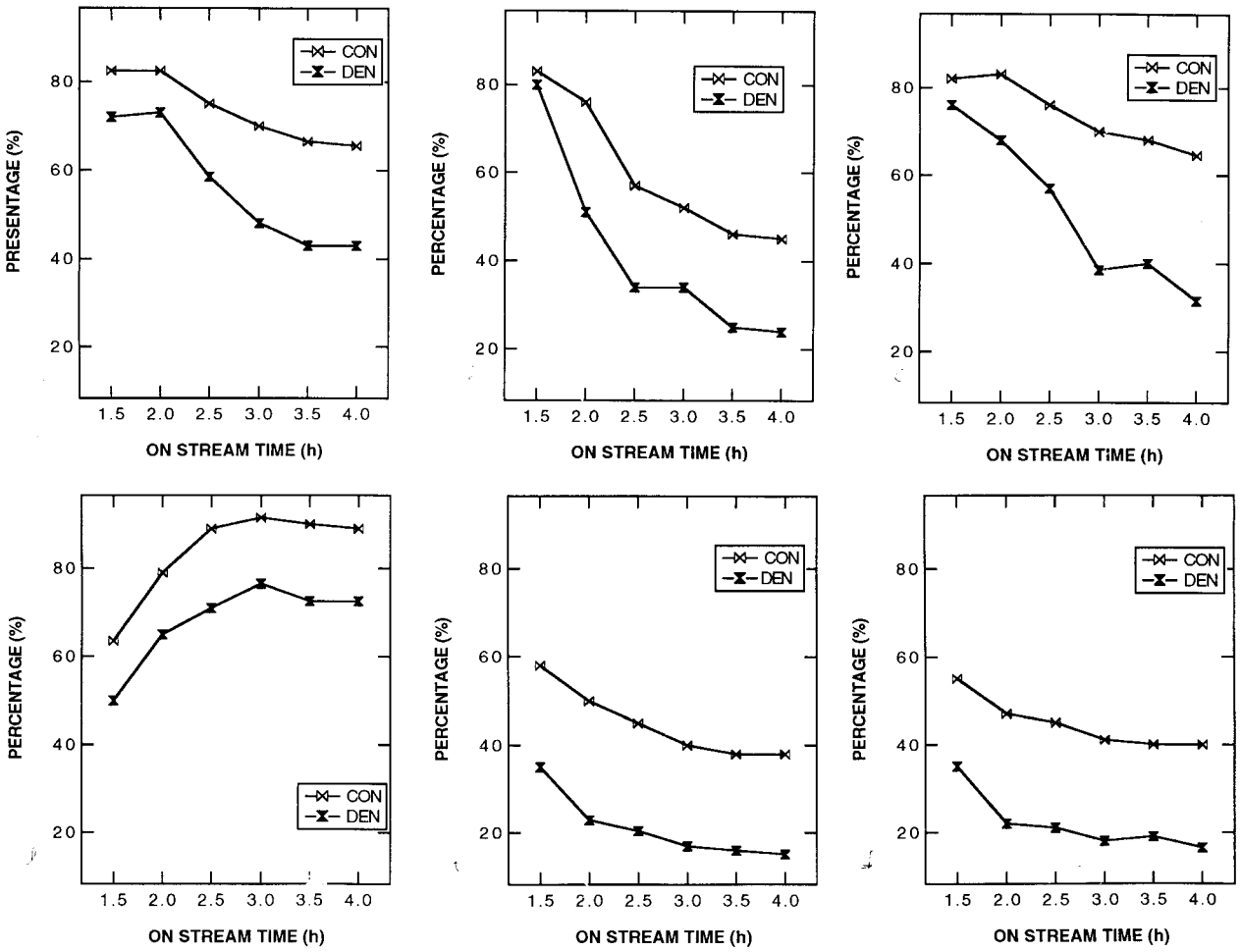

Figure 1. The conversion (CON) and the denitrogenation (DEN) of pyridine hydrodenitrogenation versus on-stream time with various catalysts. Reaction temperature 573 K, LHSV = 12 h^{-1}, H_2/oil = 300, p_{H_2} = 3.0 MPa. (a) Ti–Mo, (b) Zr–Mo, (c) Ce–Mo, (d) Co–Mo, (e) γ-Mo_2N, (f) commercial sulfided $CoMo/Al_2O_3$.

Figure 2 compares the activities of the catalysts tested after 4 h on stream. The pure γ-Mo_2N displays similar behaviour as the commercially used catalyst, while all the bimetallic nitrides show superior properties. In particular the Co–Mo catalyst displays excellent activity: 89% CON and 72.5% DEN, which is much higher than that shown by the commercial catalyst (40% CON and 16.5% DEN). Effluent analysis shows that the products from all the catalysts are similar: alkanes, of which pentane is the most abundant one, piperidine, and N-pentylpiperidine. On this basis, a simple and straightforward reaction pathway is proposed: the benzene ring of pyridine is first hydrogenated to form piperidine, which is denitrogenated to form alkanes (C_nH_{2n+2}, $n \leqslant 5$). The piperidine and pentane produced can react further to form N-pentylpiperidine.

We have recently reported [15] that, under similar experimental conditions, the catalytic properties of Zr–Mo catalysts for the hydrogenation of cyclohexene and benzene, and for the hydrodesulfurization of thiophene are better compared to those of γ-Mo_2N and the commercial catalyst, sulfided $NiCoMo/Al_2O_3$. We, therefore, conclude that the introduction of a second metal component into molybdenum nitride can significantly modify its catalytic properties, and may provide a promising method for improving the early transition metal nitrides and carbides as catalysts.

In the following sections we present DTA, SEM and XRD data on the characterization of the Zr–Mo and Co–Mo bimetallic catalysts, representing the lowest and highest catalytic activities of the bimetallics studied.

3. Differential thermal analysis

The differential thermal analysis (DTA) experiments were carried out with a DT-20B thermal analyzer (Shimadzu). 65 mg of catalyst was loaded in a crucible and a flowing mixture of N_2 and NH_3 (1 : 1 by volume, 30 ml/min) and a heating rate of 10 K/min were used.

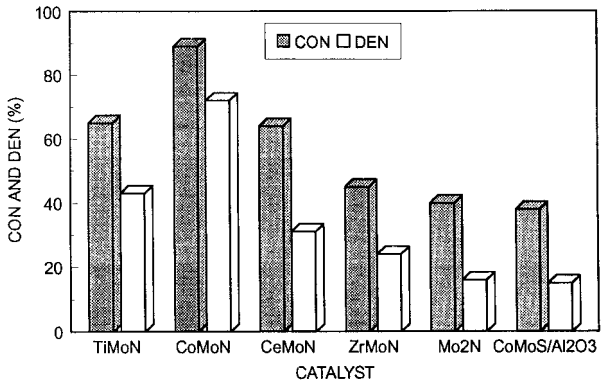

Figure 2. The conversion (CON) and denitrogenation (DEN) of pyridine hydrodenitrogenation with various catalysts after 4 h on stream. Reaction temperature 573 K, $p_{H_2} = 3.0$ MPa.

Figures 3b and 3c show the DTA results for the nitriding of the Co–Mo and Zr–Mo bimetallic precursors and figure 3a shows the results for pure MoO_3. There are four endothermic peaks and one exothermic peak in figure 3a for Mo_2N, which we have assigned elsewhere [15] as follows: the first endothermic peak is due to the dehydration of the lattice water in MoO_3; the second is due to the transformation of Mo^{6+} to Mo^{5+}; the third due to the disproportionation reaction of $2Mo^{5+}$ to $Mo^{6+} + Mo^{4+}$; the exothermic peak is attributed to the transformation of Mo^{6+} to Mo^{4+}; and, finally, the last endothermic peak is due to the nitridation reaction. The differential thermal changes during the nitriding of Co–Mo and Zr–Mo bimetallic precursors show a number of similarities to the behaviour exhibited by MoO_3, however minor variations are also observed. All three curves show the endothermic peak due to the dehydration of the lattice water, the exothermic peak due to the transformation of Mo^{6+} to Mo^{4+}, and the broad endothermic peak from nitridation. However, no peaks due to the transformation of Mo^{6+} to Mo^{5+} and from the disproportionation reaction are observed for the Co–Mo precursor. For the Zr–Mo precursor, the exothermic peak due to the transformation of Mo^{6+} to Mo^{4+} appears earlier at 658 K (figure 3c) instead of at 755 K observed for Mo_2N

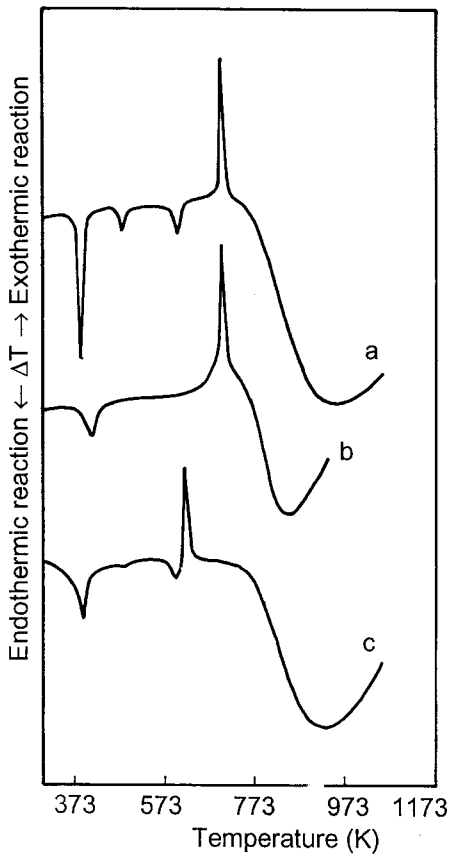

Figure 3. Differential thermal analysis of (a) MoO_3, (b) Co–Mo precursor, and (c) Zr–Mo precursor.

(figure 3a) and for Co–Mo (figure 3b). In addition, the third endothermic peak due to the disproportionation reaction of Mo^{5+} shifts from 653 K for Mo_2N in (a) to 623 K for Zr–Mo in (c). Finally for the peaks that are observed in all three cases, some intensity variation is observed. For example, the integrated area of the endothermic DTA peak for nitriding is smaller for the bimetallic precursors than pure MoO_3, indicating that the introduction of the second component makes the nitriding process easier.

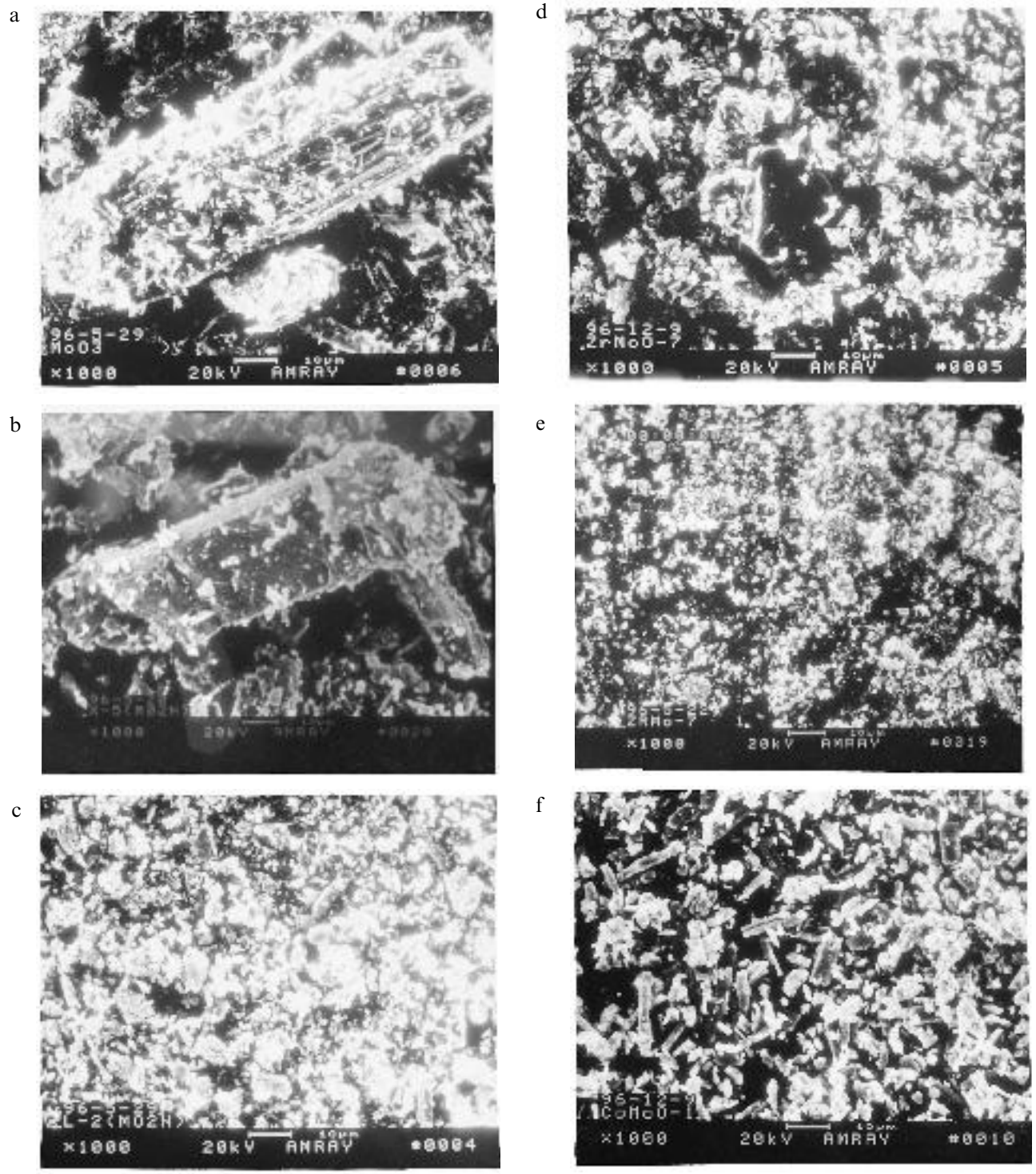

Figure 4. The surface morphology studied by scanning electron microscopy (SEM). (a) MoO_3, (b) high surface area Mo_2N ($S_{BET} = 140\ m^2/g$), (c) low surface area Mo_2N ($S_{BET} = 32\ m^2/g$), (d) Zr–Mo precursor, (e) Zr–Mo catalyst, (f) Co–Mo precursor, and (g) Co–Mo catalyst.
(Continued on next page.)

g

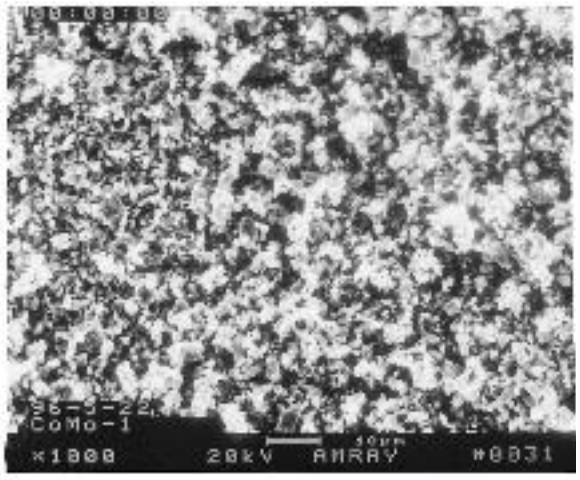

Figure 4. (Continued.)

4. Scanning electron microscopy

The surface morphology of the samples was examined using a KYKY 1000B scanning electron microscope (SEM). Before the experiment the sample was ground in a mortar and then deposited on a circular copper slide that had been coated with a gold film. The working voltage of the machine is 20 kV and a magnification of 1000 times was used. In figure 4 the micrographs of some of the precursors and the end-catalysts are compared. Figure 4a shows the morphology of MoO_3 and figures 4b and 4c show the morphologies of high surface area Mo_2N ($S_{BET} = 140\ m^2/g$) and low surface area Mo_2N ($S_{BET} = 32\ m^2/g$), respectively. Clearly the morphologies in figures 4a and 4b are very alike, which is consistent with the assumption that the nitridation from MoO_3 to high surface area Mo_2N is a topotactic reaction [11]. The morphologies in figures 4a and 4c are very different, which is consistent with the opinion of a number of authors [16,17] that the transformation of MoO_3 to low surface area Mo_2N may not be a topotactic reaction. Figures 4d and 4e show the morphologies of the Zr–Mo material before and after nitridation, and figures 4f and 4g show those of the Co–Mo material before and after nitridation, respectively. It is clear that the morphologies of the precursors, figures 4d and 4f, bear little similarity with that of MoO_3 (a). This clearly suggests that the introduction of the second metal components by coprecipitation leads to significant alteration and disruption of the platelet structure of MoO_3.

5. Powder X-ray diffraction

The XRD work was performed by using a Rigaku Rotaflex (Ru-200B) powder X-ray diffractometer equipped with a Cu target and Ni grating monochromatic system. The working voltage of the instrument was 40 kV and the electric current used was 50 mA. The samples were ground gently and fixed on a backless glass slide for the experiment.

In figure 5 the XRD profiles for the Zr–Mo bimetallic material, before and after nitridation, (a) and (b), are compared with the XRD profiles of MoO_3 (c), γ-Mo_2N (d), ZrO_2 (e), $ZrMo_2O_8$ (f), and $ZrMo_2N_x$ (g). $ZrMo_2O_8$ was prepared by mixing zirconium nitrate and ammonium heptamolybdate in an aqueous solution with a stoichiometric Zr/Mo ratio of 1 : 2 and evaporating it in a water-bath, followed by drying at 393 K for 2 h and calcining at 773 K for 3 h. $ZrMo_2N_x$ is the nitridation product of the $ZrMo_2O_8$, obtained under the nitriding conditions mentioned in section 1. Comparison of figure 5a with figures 5c, 5e, and 5f suggests that the crystalline component of the Zr–Mo precursor is largely composed of MoO_3 and $ZrMo_2O_8$. However, of the peaks that can be unambiguously assigned to MoO_3, an altered intensity of the diffraction peaks is observed, suggesting an alteration in MoO_3 structure, with a lower concentration of {010} planes and a greater preponderance of (110) and (021) planes. It should be noted that the weak intensity of the other residual diffraction peaks makes it difficult to ascertain the presence of crystalline ZrO_2 in the Zr–Mo precursor.

After nitridation of the bimetallic precursor, only features arising from Mo_2N are detectable in the XRD data of the final resultant catalyst materials, figures 5b and 5d. Unfortunately, the XRD profile of $ZrMo_2N_x$

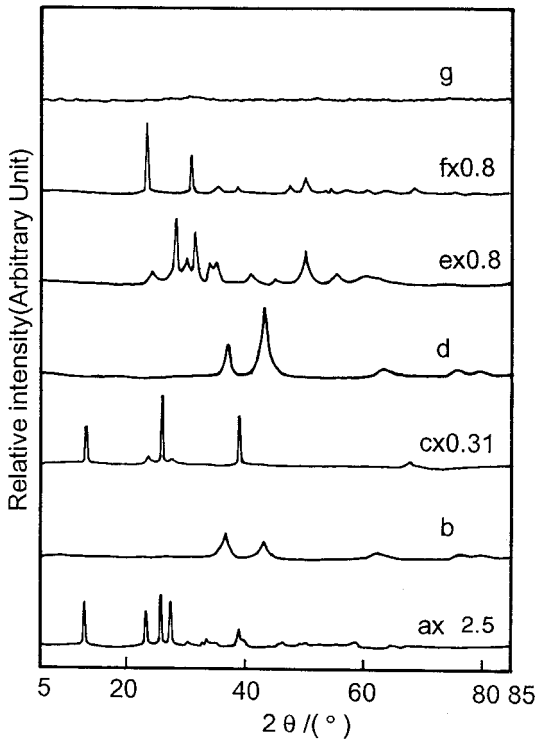

Figure 5. XRD profiles of Zr–Mo series. (a) Zr–Mo precursor, (b) Zr–Mo catalyst, (c) MoO_3, (d) γ-Mo_2N, (e) ZrO_2, (f) $ZrMo_2O_8$, (g) $ZrMo_2N_x$.

(figure 5g) is featureless and therefore cannot provide any indication for the existence of the bimetallic nitride in the Zr–Mo catalyst. However, it is significant to note that the intensity order between diffractions from the (111) and (200) Mo_2N planes in the Zr–Mo catalyst is reversed from that of high surface area Mo_2N, where the topotactic nitriding reaction [5,11,18] brings about the crystallographic orientation relationship of $(010)_{MoO_3}\|(100)_{Mo_2N}$, leading to a more intense (200) peak than the (111) peak. We note that Ramanathan and co-workers also observed an altered intensity order in their XRD experiments with bimetallic nitrides, but no explanation was offered [17]. Our XRD data, figures 5a and 5c, clearly show that this difference can be attributed to the fact that the MoO_3 component in the coprecipitated bimetallic precursors has a different morphology in which the dominance of the {010} planes is disrupted and where (110) and (021) planes are present in significant amount.

In figure 6 the XRD profiles of the Co–Mo bimetallic material, before and after nitridation, are compared ((a) and (b)). The XRD profiles of some other materials are also displayed for comparison purposes: MoO_3 (c); γ-Mo_2N (d); CoO (e); $Co_2Mo_3O_8$ (f); $CoMoO_4$ (g); and $Co_2Mo_3N_x$ (h). $Co_2Mo_3O_8$ and $CoMoO_4$ were prepared in a similar way as $ZrMo_2O_8$; $Co_2Mo_3N_x$ was obtained

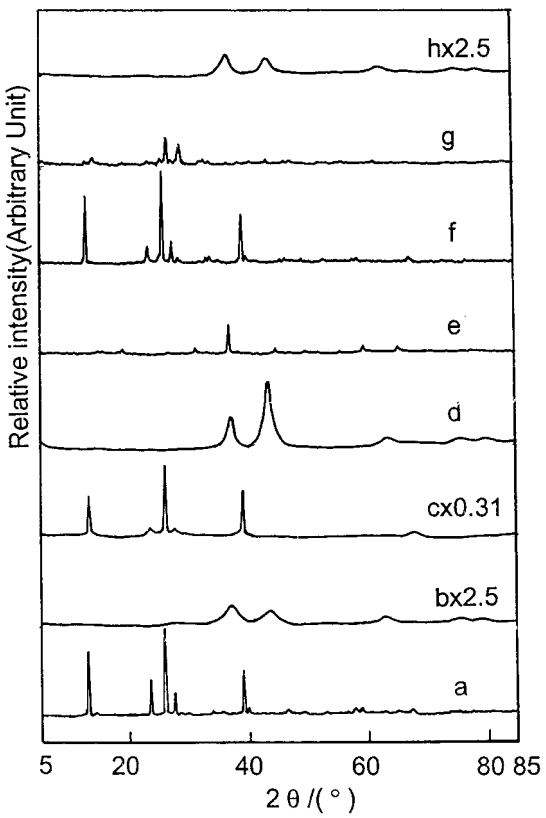

Figure 6. XRD profiles of Co–Mo series. (a) Co–Mo precursor, (b) Co–Mo catalyst, (c) MoO_3, (d) γ-Mo_2N, (e) CoO, (f) $Co_2Mo_3O_8$, (g) $CoMoO_4$, (h) $Co_2Mo_3N_x$.

by nitriding $Co_2Mo_3O_8$ under identical conditions as used with MoO_3. The XRD profile of the bimetallic Co–Mo precursor with 3 wt% Co oxide, figure 6a, resembles the diffractions of MoO_3 and $Co_2Mo_3O_8$, figures 6c and 6f. Since the profile of $Co_2Mo_3O_8$ is almost identical to that of MoO_3 it is difficult to distinguish the monometallic phase from the bimetallic one. However, given that the precursor only contains 3% Co by weight, it can not simply consist of the $Co_2Mo_3O_8$ phase and we suggest that a significant amount of MoO_3 must also be present. No CoO features, figure 6e, are seen for the bimetallic precursor and the weak intensity of the residual peaks makes it difficult to analyse for the presence of $CoMoO_4$. We, therefore, conclude that the bimetallic precursor of Co–Mo catalyst is a mixture of MoO_3 and $CoMo_3O_8$.

After nitriding the Co–Mo precursor, all the features due to MoO_3 and $CoMo_3O_8$ disappear and only the features attributable to Mo_2N and $Co_2Mo_3N_x$ remain. However, as with the Zr–Mo catalyst, both the bimetallic catalyst and $Co_2Mo_3N_x$ display an intensity order that is reversed with respect to that of Mo_2N, with the (111) signal more intense than the (200) diffraction. Again, as for the Zr–Co catalyst, upon the introduction of the second metal component into MoO_3 by coprecipitation, all the XR diffractions from the {0k0} planes of MoO_3 are dramatically weakened. If the topotactic transformation, $(010)_{MoO_3}\|(100)_{Mo_2N}$, still holds for the bimetallic catalyst, then a consequent weakening of the XR diffraction from the (200) plane of the nitrided Co–Mo catalyst would be expected.

6. Summary

In this work we have succeeded in producing a coprecipitation method for the preparation of bimetallic precursors, which introduces a second metal component into the subsequently produced high surface area nitrides. The synthetic conditions are less demanding than those necessary for the preparation of Mo_2N from MoO_3. Under the reaction conditions used in this research, the bimetallic catalysts showed better catalytic properties than pure γ-Mo_2N and the commercially used catalyst for hydrodenitrogenation of pyridine. Although the underlying reasons for the effect of the second component in improving the catalytic properties of Mo_2N are not clear at present, we make the following observations based on our characterization work.

First, XRD results show that the characteristic platelet morphology of MoO_3, favouring the formation of {0k0} planes, is damaged upon the introduction of the second metal component by coprecipitation; this conclusion is further supported by SEM data. There is a strong decrease in concentration of the {010} orientated planes of MoO_3 and, even at low Zr and Co content, the diffractions from the {0k0} planes of MoO_3 ($2\theta = 12.7°$: (020);

25.7°: (040); 39.0°: (060)) decrease dramatically in intensity. Meanwhile the other diffractions of MoO_3, e.g. from the (021) plane ($2\theta = 27.3°$) and the (110) plane ($2\theta = 23.3°$), are present in greater relative intensity compared to pure MoO_3. This is reminiscent of the behaviour reported for intermediate phases formed during the reduction of MoO_3 in which crystallographic shear occurs, causing oxygen vacancies to collapse along {120} shear planes [18]. The alteration in the MoO_3 morphology leads to a Mo_2N phase where the intensity of the Mo_2N (200) plane is now lower than that of (111) planes. The HDN reaction on molybdenum nitrides has been shown to be structure sensitive [20,21] and the enhanced activity of the bimetallic phase could arise from the different activities of (200) and (111) planes, with the latter perhaps being more active. Alternatively, defect sites have been implicated as active catalytic centres in nitrides [21] and the collapse of the platelet structure will almost certainly increase the concentration of the boundary and grain sites. Finally the electronic effect of introducing foreign atoms into Mo_2N also needs to be considered since a change in the electron density distribution and the d-band structure will certainly modify the catalytic behaviour. Some evidence for the importance of this is provided by a comparison of Zr–Mo and Co–Mo catalysts. XRD data for both catalysts show strong similarities, however each catalyst exhibits rather different activity versus time profiles, figure 1, clearly indicating that the individual chemical promotion brought about by the introduction of the second metal component is also important in governing the catalytic behavior. At present, however, it is not possible to further speculate on the exact nature of this chemical promotion.

Acknowledgement

The authors are grateful to the Research Institute of Petroleum Processing of the SINOPEC, the K.C. Wong Fellowships and the British Council for their valuable financial support. The authors are also grateful to Professor E.G. Derouane of the Leverhulme Centre for useful discussion.

References

[1] G.S. Ranhotra, A.T. Bell and J.A. Reimer, J. Catal. 108 (1987) 40.
[2] L. Leclercq, K. Imura, S. Yoshida, T. Barbee and M. Boudart, in: *Preparation of Catalysts II*, ed. B. Delmon (Elsevier, Amsterdam, 1978) p. 627.
[3] M. Boudart, S.T. Oyama and L. Leclercq, in: *Proc. 7th Int. Congr. on Catalysis*, Vol. 1, Tokyo 1980, eds. T. Seiyama and K. Tanabe, p. 578.
[4] J.C. Schlatter, S.T. Oyama, J.E. Metcalfe III and J.M. Lambert Jr., Ind. Eng. Chem. Res. 27 (1988) 1648.
[5] E.J. Markel and J.W. Van Zee, J. Catal. 126 (1990) 643.
[6] H. Abe and A.T. Bell, Catal. Lett. 18 (1993) 1.
[7] F.H. Ribeiro, R.A. Dalla Betta, M. Boudart, J. Baumgartner and E. Iglesia, J. Catal. 130 (1991) 86.
[8] F.H. Ribeiro, M. Boudart, R.A. Dalla Betta and E. Iglesia, J. Catal. 130 (1991) 498.
[9] B. Dhandapani and S.T. Oyama, Catal. Lett. 35 (1995) 353.
[10] M.J. Ledoux, C. Pham-Huu and R.R. Chianelli, Current Opinion in Solid State & Materials Science 1 (1996) 96.
[11] L. Volpe and M. Boudart, J. Phys. Chem. 90 (1986) 4874.
[12] R.S. Wise and E.J. Markel, J. Catal. 145 (1994) 335.
[13] C.H. Jaggers, J.N. Michaels and A.M. Stacy, Chem. Mater. 2 (1990) 150.
[14] Y. Zhang, Z. Wei, W. Yan, P. Ying, C. Ji, X. Li, Z. Zhou, X. Sun and Q. Xin, Catal. Today 30 (1996) 135.
[15] Y. Zhang, Y. Li, R. Raval, C. Li, R. Zhai and Q. Xin, J. Mol. Catal., submitted.
[16] J.G. Choi, R.L. Curl and L.T. Thompson, J. Catal. 146 (1994) 218.
[17] S. Ramanathan, C.C. Yu and S.T. Oyama, Preprints of Papers, American Chemical Society, Division of Fuel Chemistry 40 (1995) 998.
[18] L. Volpe and M. Boudart, J. Solid State Chem. 59 (1985) 332.
[19] W.F. McClune, in: *Powder Diffraction File, Inorganic Compounds*, JCPOS (Swarthmore 1980) pattern 5-0508.
[20] J. Choi, J.R. Brenner, C.W.Colling, B.G. Demczysk, J.L. Dunning and L.T. Thompson, Catal. Today 15 (1992) 201.
[21] J.G. Choi, H.J. Lee and L.T. Thompson, Appl. Surf. Sci. 78 (1994) 299.